Journal of Catalysis **188,** 90–101 (1999)
Article ID jcat.1999.2600, available online at http://www.idealibrary.com on IDEAL®

Skeletal Isomerization of Hexenes on Tungsten Oxide Supported on Porous α-Alumina

V. Logie,*[,1] G. Maire,* D. Michel,† and J.-L. Vignes†

*LERCSI, UMR 7515 du CNRS, Université Louis Pasteur, 25 rue Becquerel, BP 08, 67087 Strasbourg Cedex 2, France; and †CECM, UPR 2801 du CNRS, 15 rue Georges Urbain, 94407 Vitry-sur-Seine, France

Received March 8, 1999; revised June 9, 1999; accepted June 9, 1999

The isomerization of hexenes on tungsten oxide supported on a porous α-Al_2O_3 catalyst with a coverage approaching one monolayer has been studied. The support used is a porous monolith of α-alumina prepared by a novel method. It appears that this catalyst exhibits high and very stable activity and isomerization selectivity under a hydrogen stream at 350°C or at higher temperatures. No pretreatment is necessary to induce the activity. The skeletal isomerization proceeds only through an acidic mechanism including carbenium ion rearrangements. The catalyst was characterized by XPS, XANES, XRD, and TPR. The acidic character of the fresh calcined surface was attributed to the presence of amorphous tungsten oxide species in interaction with the support, as Lewis acidic sites, and to the presence of OH groups as Brønsted acidic sites. Such a catalyst has less resistance to poisoning by carbonaceous residues at low temperature (200°C), but is fully rejuvenated by a simple exposure to hydrogen at 350°C.

Key Words: **WO_3/α-Al_2O_3; hexenes isomerization; acidic mechanism; XPS; XANES; TPR; XRD.**

INTRODUCTION

The groups of Boudart *et al.* (1–3) and Maire *et al.* (4–7) reported that tungsten carbides modified by oxygen are highly selective catalysts for hydrocarbon isomerization through a bifunctional mechanism, where the carbide induces the dehydrogenation–hydrogenation of hydrocarbons, while the WO_x species formed on the surface performs the skeletal isomerization of alkenes through an acidic mechanism including carbocations. However, these oxygen-modified tungsten carbide catalysts are sensitive to carbonaceous residues formed during the reaction, and deactivation always occurs.

More recently Maire *et al.* (8–10) have shown that in certain conditions of time, temperature, and hydrogen or hydrocarbon pressure, bulk tungsten oxides (WO_3, WO_2) could give very selective catalysts for the isomerization of hexanes and hexenes. However, these systems deactivate under the reaction stream, and the catalytic properties are widely modified under hydrogen flow as a function of time and temperature because of the continuous reduction of the surface from WO_3 to metal (W) via intermediate tungsten oxide phases $W_{20}O_{58}$, WO_2, and W_3O.

Many data in the literature reported that for supported WO_3/Al_2O_3 the interaction between tungsten oxide and alumina has a pronounced effect on the properties of the supported tungsten oxide phase (11–16). At monolayer coverage or less, the WO_3/Al_2O_3 catalysts were found to be active and selective for alkene isomerization reactions (17–19). Baker *et al.* (18–20) have shown that, for equivalent tungsten oxide loading, α-Al_2O_3 is a better catalyst support than γ-Al_2O_3 because of its higher basic character. They proposed that catalytic activity for alkene isomerization reactions takes place on the partially reduced tungsten oxide species, which is stabilized by a weak interaction with the alumina, associated with OH acidic sites at the surface. Ponec *et al.* (17, 21), who studied 1-butene isomerization, observed that the selectivity in isobutene product and the stability of the catalyst depend strongly on the tungstate loading and therefore on the structure of the surface tungsten oxide species. They revealed that an increase in skeletal isomerization occurs when dimeric WO_4^{2-} species become abundant at the catalyst surface. The above considerations show that the nature of the reaction sites is not yet well defined.

The WO_3/Al_2O_3 system with monolayer coverage or less has been examined with a variety of characterization techniques, XPS (11, 13–15, 19, 20, 22), LRS (11, 14, 16, 22–24), XANES (25), ISS (14, 20), TPR (23, 26), and IR (21, 27). It has been shown that, for submonolayer systems, the supported tungsten oxide phase is present as an amorphous surface complex coordinated to the alumina support which is much more difficult to reduce than bulk WO_3. Furthermore, the reduction of these amorphous tungsten oxide species in metal tungsten (W) occurs in one step, unlike bulk WO_3 which is reduced into W^0 via W^{5+} and W^{4+}. However, despite the large amount of work on this system, the structure

[1] To whom correspondence should be addressed. Fax: 00-33-88-13-68-69. E-mail: monstre@chimie.u-strasbg.fr.

0021-9517/99 $30.00

of these alumina-supported surface tungsten oxide species is still under discussion. One group has proposed that it consists of bridged distorted octahedral tungsten species (16, 23) while other groups have proposed the formation of mono- or di-WO_4^{2-} species tetrahedrally coordinated, as a function of the tungsten loading (11, 14, 17, 19, 21, 22, 24–27). In these works, γ-alumina is mainly used as support, and other aluminas, such as α-Al_2O_3, are scarcely investigated (18–20).

In this work, we present the catalytic activity for hexene isomerization on a WO_3/α-Al_2O_3 system with a coverage of tungsten oxide approaching a monolayer. The support used is a porous monolith of α-Al_2O_3 prepared by a novel method described in (28, 29). As α-alumina was scarcely used as support for tungsten oxide, it is of value to examine its ability to favour the formation of the active species for alkene isomerization as proposed by Baker (18–20). We establish a correlation between the catalytic behaviour of this WO_3/α-Al_2O_3 system and the textural and structural properties of the surface tungsten oxide species determined by different techniques of characterization (XPS, XANES, TPR, XRD, and *in situ* area measurements).

EXPERIMENTAL

Catalyst Preparation

The α-alumina used as a support for our tungsten-oxide-based catalysts was prepared with a method described by Vignes *et al.* (28). Highly porous monoliths of amorphous hydrated alumina are thus obtained by direct oxidation of aluminum plates without metal passivation. After an adequate temperature treatment, γ, θ, or α porous alumina monoliths can be obtained (28). The α-alumina used was obtained at 1200°C.

The tungsten oxide catalyst was prepared by impregnating the α-Al_2O_3 support with an aqueous solution of sodium tungstate (0.45 mol/liter and pH ~5) using the method described by Baker *et al.* (18). The sample was first dried in a vacuum desiccator for ~2 h and then washed with a nitric acid (2.2×10^{-2} mol/l) solution by decantation (~1 h) to remove sodium nitrate. Washing was repeated three times and the catalyst was finally dried at 200°C for 4 h in air. A catalyst containing 6.7 wt% WO_3, named 6.7WA, was prepared at a composition corresponding, according to previous studies (11, 22), to a WO_3 monolayer coverage.

Catalyst Characterization

The surface area of the catalyst was measured by the BET method using a Coulter SA instrument, Model 3100. The standard pretreatment consisted of heating the sample under dynamic vacuum at 250°C for 1 h to remove water and other impurities. The measurement was made at liquid nitrogen temperature with nitrogen as the adsorbate gas.

The crystalline structure was analyzed by X-ray diffraction (XRD) using a Siemens Model D-500 diffractometer with Cu $K\alpha$ radiation ($\lambda = 1.54$ Å). All diffractograms were compared with those of the JCPDS data file for identification.

The microstructure features of the α-alumina monolith were studied by SEM using a Zeiss 950DSM apparatus.

The XP spectra were obtained using an ESCA III VG instrument with Al $K\alpha$ radiation ($E_c = 1498$ eV). The treatments under hydrogen were done *in situ* with conditions similar to those for the catalytic experiments in terms of pressure and temperature of reduction (450°C). The method developed in our laboratory for deconvolution of the XP spectra (29) was used. In this work, all binding energies were referred to the Al2*p* at 74.6 eV. The spin–orbit coupling is 2.2 ± 0.2 eV. The intensity ratio between W4$f_{5/2}$ and W4$f_{7/2}$ signals adopted for all tungsten oxidation states were close to the theoretical value (0.75). Binding energies are reported within an experimental error of ±0.2 eV.

Tungsten reducibility was determined by temperature-programmed reduction (TPR) using an XSORB (IFP-Gira) apparatus. Five percent H_2/Ar, purified on molecular sieves, was used as a reducing agent, with a 25 cc/min flow. H_2 consumption was measured by means of a catharometric detector. One hundred milligrams of sample were placed in a quartz reactor. After an *in situ* pretreatment in air at 400°C for 2 h, the temperature was increased at the rate 8°C/min up to 900°C where it remained steady for 2 h. The oxidizing treatment in air at 400°C and the TPR measurements were repeated two times. The selection of these experimental operating variables leads, for the 6.7WA sample, to the values $K = 35$ s and $P = 4.6$ K, where K and P are the characteristic numbers defined, respectively, by Monti and Baiker (30) and Malet and Caballero (31) to obtain optimum reduction profiles. We can note that the K value is inferior to the inferior limit of 50 s but the P value is well inferior to 20 K, which is the maximum value determined by the authors (31). On the other hand, the values of these K and P parameters for the WO_3 sample are, respectively, 518 s and 69 K, which is superior to the limits values. These differences are due to the fact that we decided to perform the TPR experiments under the same experimental conditions for the two catalysts.

XAS experiments were carried out at the Orsay Synchrotron Radiation Laboratory (LURE) on the DCI EXAFS4 beam line. The storage ring operating conditions were 1.85 GeV with an average current of 250 mA. XAS spectra were collected in the transmission mode using a double-crystal Si(311) monochromator at the L_I-edge of tungsten. Energy was calibrated using Au polycrystalline foil placed behind the sample. XANES spectra of WO_3, WO_2, W(0), and Na_2WO_4 were recorded as references. *In situ* XANES data for the 6.7WA sample were obtained

at room temperature under an H_2 stream and at 450°C after reduction under hydrogen at this temperature.

The XANES spectra were normalized using the Michalowicz procedure (32) by fitting to the pre-edge data, fitting a polynomial spline to the data of the EXAFS region, extrapolating both functions to zero energy, taking the difference, and normalizing the data unit step height.

Catalytic Procedures

Catalytic reactions were carried out in an all-glass micropilot working at atmospheric pressure. The device was equipped with a flow meter, a reactor working as a fixed bed, and a double thermal conductivity detector system (TCD) recording the partial pressure of the reactant (provided by a saturator) before and after the reactor. Reactions were performed at 350°C with an H_2 flow of 54 cc/min. Particular attention has been given to the purification of the reaction gases and of the tested hydrocarbons. The H_2 flow is led over Pt/Al_2O_3 catalyst to convert the residual oxygen water. The formed water is trapped by zeolites. In order to make sure that all oxygen has been removed, the reaction gases are led over a green MnO bed which becomes black (MnO_2) if some oxygen is still present. Around 15 mg catalyst is introduced onto the quartz frit in the reactor. Four hexenes have been tested, 4-methyl-1-pentene (4M1Pene), 1-hexene (1Hene), methylcyclopentene-1 (MCPene), and cyclohexene (CHene). The hydrocarbon is introduced via a septum and then drawn into the saturator which is immersed in a cooling bath whose temperature is adjusted and maintained constant, in order to have the following pressure ratios: $p(4M1Pene)/p(H_2) = 9.7/750.3$; $p(1Hene)/p(H_2) = 5.1/754.9$; $p(MCPene)/p(H_2) = 3.4/756.6$; $p(CHene)/p(H_2) = 6.0/754.0$. The reaction products are hydrogenated before being sampled with an air-tight syringe and analyzed by gas chromatography with a FID.

RESULTS AND DISCUSSION

Surface Area Determination

The BET surface area of the support α-Al_2O_3 is relatively high (~44 m^2/g). The BET surface area of the catalyst 6.7WA measured after the calcination treatment at 200°C is around 40 m^2/g. No evolution of this surface area was detected after treatment under H_2 at 450°C for 12 h in the catalytic micropilot.

XRD and SEM Measurements

The α-alumina monolith used as support has a grain size about 300 nm as deduced from SEM data (Fig. 1).

The XRD pattern of the 6.7WA catalyst after the calcination treatment at 200°C is given in Fig. 2. The support is a well-crystallized α-alumina phase with some traces of θ-alumina. No tungsten oxide diffraction peak is observed. The significant increase of the background profile observed in the 2θ region between 15° and 40° indicates the tungsten species of the 6.7WA catalyst are amorphous or nanocrystalline.

XPS Analysis

The XP spectra of the W4*f* region of the 6.7WA catalyst before and after *in situ* treatments under hydrogen are presented in Fig. 3. After the calcination treatment, the spectrum of the 6.7WA sample reveals that the only oxidation state present at the surface is hexavalent tungsten (Fig. 3a). The W4*f* linewidth (FWHM) is somewhat larger for the 6.7WA sample than for WO_3. These W^{6+} species are characterized by the W4$f_{7/2}$ binding energy at 36.0 eV, like hexavalent tungsten in the $Al_2(WO_4)_3$ compound (33), while the binding energy of the W^{6+} in the bulk WO_3 compound was determined at 35.5 eV (8). Despite the coincidence between the W4*f* peaks in $Al_2(WO_4)_3$ and the 6.7WA calcined catalyst, the XRD results (Fig. 2) lead us to the conclusion that bulk $Al_2(WO_4)_3$ is not formed on the 6.7WA catalyst under our conditions of calcination. This result is in agreement with many data (13, 14, 16, 19, 22–26, 34) concerning the characterization of supported tungsten oxide on alumina when the WO_3 loading is below one monolayer. Indeed, these previous investigations reveal that bulk $Al_2(WO_4)_3$ formation is possible with temperature treatment above 1100°C. The difference in W^{6+} binding energy and in W4*f* linewidth, observed between the 6.7WA and WO_3 catalysts, may also be ascribed to the presence of a strong interaction between tungsten oxide species and alumina support and/or to a difference in tungsten coordination. The W atoms in the WO_3 are thus octahedrally coordinated while in the $Al_2(WO_4)_3$ the W^{6+} ions are tetrahedrally coordinated. Despite the structure of the surface, tungsten oxide species cannot be exactly determined by XPS; these observations concerning the W^{6+} binding energy present on the calcined surface of the 6.7WA catalyst suggest that hexavalent tungsten ions are not octahedrally coordinated onto the alumina surface. This is in agreement with conclusions of Baker (19), who showed the same difference, in terms of binding energy, between the W4*f* peaks in WO_3 and a 6 wt% WO_3/α-Al_2O_3 catalyst heated in air at 400°C for 20 h.

An *in situ* treatment under hydrogen at 450°C for 3.5 h at atmospheric pressure (Fig. 3b) leads to a reduction of above 22% of W^{6+} species into pentavalent tungsten. A further exposure of this sample at 450°C under hydrogen (Fig. 3c) results in the total reduction of W^{5+} into tungsten metal W^0, while the W^{6+} concentration remains constant (~78%). In Table 1, we report the evolution of the W/Al atomic ratio during the reduction treatments under hydrogen at 450°C. We can observe that the W/Al atomic ratio decreases by a factor of 2 during the reduction treatments.

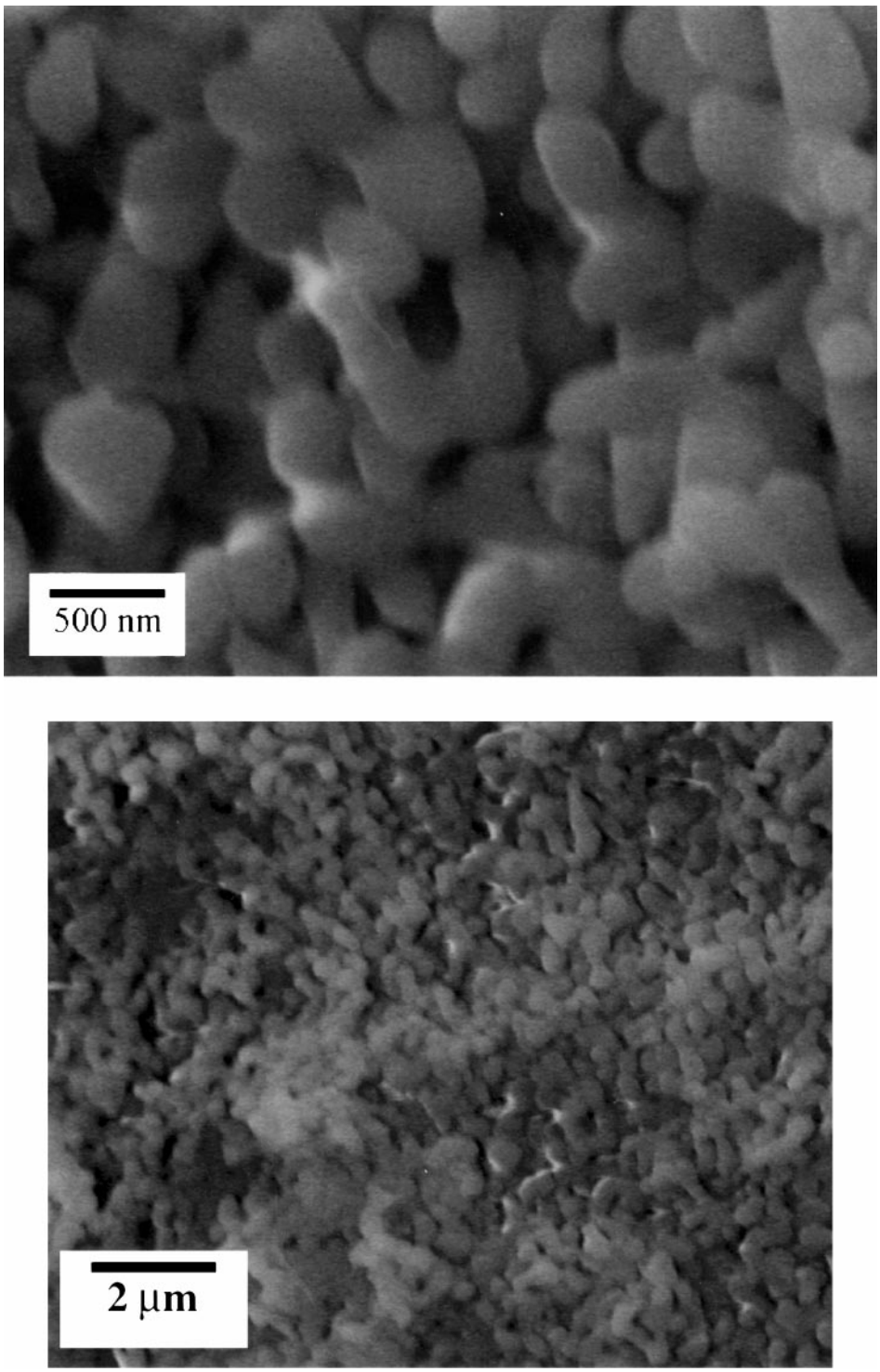

FIG. 1. SEM bright field image of α-alumina obtained after heating a hydrated alumina for 4 h at 1200°C.

Some studies, using the TPR (23, 26, 35) and the XPS (11, 13, 14) techniques, have shown that the reduction behaviour of WO_3/γ-Al_2O_3 systems depends on the surface coverage and therefore on the structure of the surface alumina-supported tungsten oxide species. Above one monolayer coverage of tungsten oxide on alumina, crystallites of WO_3 are formed (9, 22, 25), which exhibit reduction kinetics and mechanisms indistinguishable from bulk WO_3. On the other hand, at monolayer coverage or less, the supported tungsten oxide phase is present as an amorphous surface complex coordinated to the alumina support (11, 13, 14, 19, 22–25). The W^{6+} species which constitute the amorphous layer

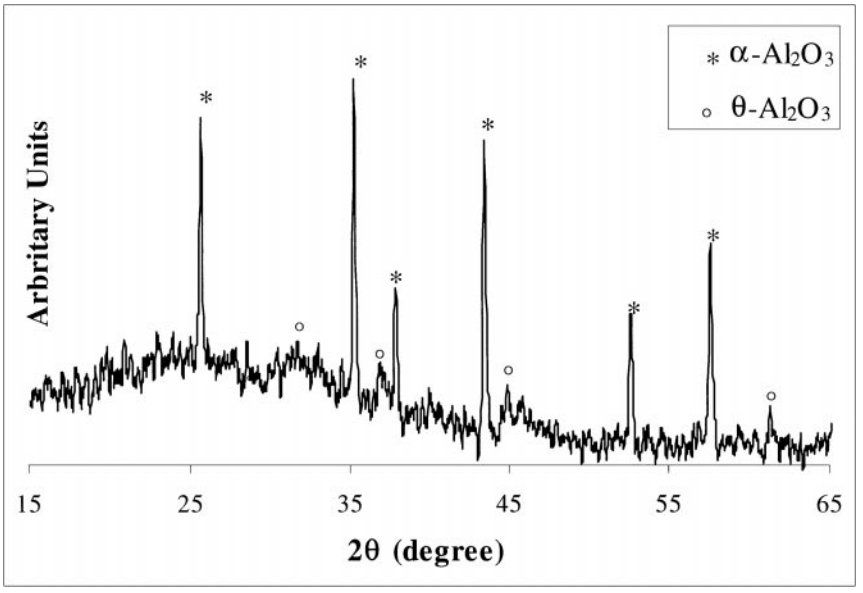

FIG. 2. XRD pattern of the 6.7WA catalyst after calcination in air at 200°C for 4 h.

require a temperature higher than 550°C to be reduced and their reduction to metal (W^0) is made without formation of W^{5+} and W^{4+} intermediates, unlike for bulk WO_3 (11, 14, 22, 26). On the basis of these considerations, the W^{5+} and W^0 species observed by XPS after a treatment of the 6.7WA sample under hydrogen at 450°C were assigned to the reduction of a few WO_3 crystallites which were present on the initial fresh prepared surface. The presence of WO_3 crystallites means that the loading of 6.7 wt% WO_3 on the α-Al_2O_3 support is slightly in excess of the coverage required for the formation of a monolayer, according to the monolayer value determined by Salvati *et al.* (11) and Chan *et al.* (22). This difference in the monolayer value can be due to the nature of the alumina used as support, as α-alumina possesses less reacting hydroxyl groups than the γ-phase used by Salvati or Chan. All these observations from the surface characterization by the XPS technique lead us to the conclusion that the surface of our 6.7WA catalyst is composed, on the one hand, mainly of amorphous tungsten oxide species which strongly interact with the alumina support and are irreducible under our conditions (temperature, time, and H_2 pressure) and, on the other hand, of some WO_3 crystallites on top of the amorphous alumina-supported tungsten species which are reduced via the same mechanism and conditions as bulk WO_3.

TABLE 1

Atomic Ratio W/Al for the 6.7WA Catalyst after Calcination in Air at 200°C for 4 h and after *In Situ* Reduction by H_2 at 450°C for 3.5 h and for 7.5 h

	W/Al
Fresh	0.090
R450°C/3h30	0.060
R450°C/7h30	0.048

TPR Analysis

The TPR profiles of the 6.7WA sample are reported in Fig. 4. The first TPR profile is composed of two peaks, a small shoulder near 550°C and a larger peak at 800°C which is completed after isothermal treatment at 900°C for 1 h. Although the shape of the TPR profile suggests complete reduction, the hydrogen consumption ($\Delta RN = 1.9$) corresponds to only 63% reduction. This ΔRN value means that some tungsten oxide species require a reduction temperature higher than 900°C. The TPR profile of bulk WO_3 (Fig. 5) is totally different from those of the 6.7WA catalyst, which confirms that the supported 6.7WA catalyst is not mainly composed of WO_3 species. Bulk WO_3 is completely reduced ($\Delta RN = 2.8$) in a four-step process. This is in agreement with established kinetics for the main steps of reduction in H_2: WO_3, $WO_{3-x,(0<x<1)}$, WO_2, W, where WO_{3-x} could correspond, as a function of the reduction conditions, to a variety of suboxides ($W_{20}O_{58}$, $W_{18}O_{49}$, $W_{24}O_{68}$...) (13–15, 26, 36–39). On the basis of both the XPS and the XRD results, we assigned the shoulder near 550°C to the reduction of the few WO_3 crystallites present on top of the monolayer, in $WO_{3-x,(0<x<1)}$ oxides. The broad reduction peak at 800°C is assigned to the reduction of the amorphous tungsten oxide species anchored to the alumina and the $WO_{3-x,(0<x<1)}$ oxides to tungsten metal W. These results are

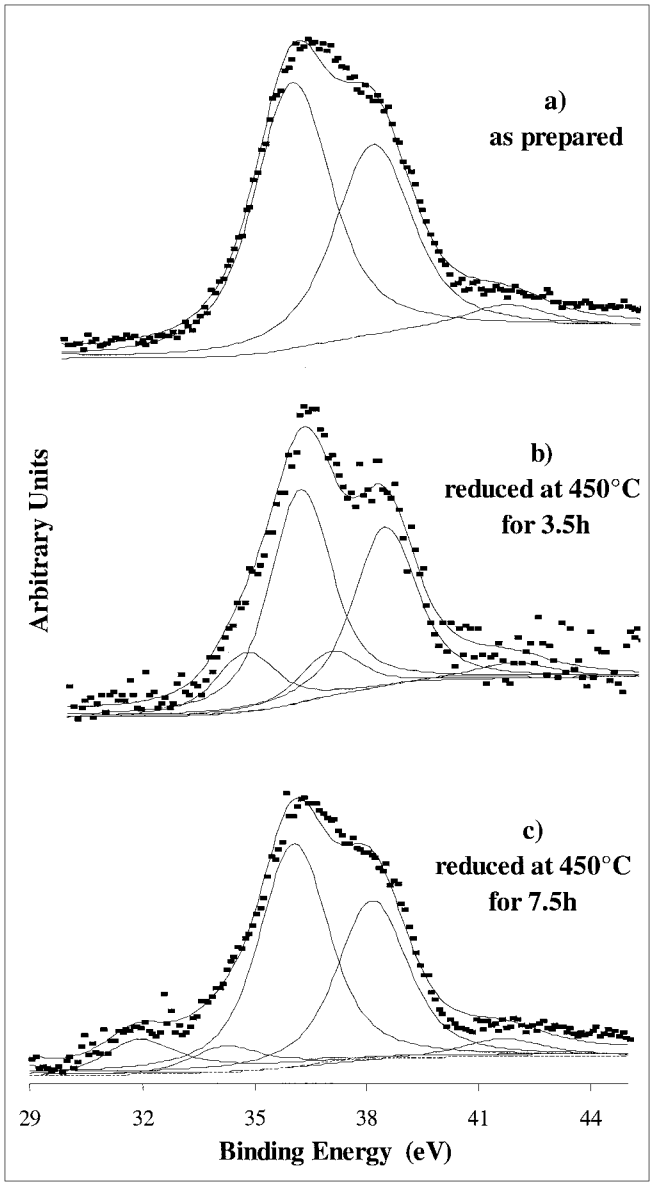

FIG. 3. XPS spectra for the 6.7WA catalyst in the W4*f* region after calcination in air at 200°C for 4 h (a) and after *in situ* reduction by H_2 at 450°C for 3.5 h (b) and 7.5 h (c).

consistent with previous studies (23, 26, 40), which examined the TPR patterns of WO_3/γ-Al_2O_3 systems at different loadings. At coverage below the monolayer, a single peak is observed at temperatures higher than 1000°C, which was assigned to the reduction of the tungsten species coordinated on the alumina support. At loading equivalent to or higher than one monolayer, a smaller additional peak appears at lower temperature (between 630 and 830°C). This second peak was attributed to the partial reduction of WO_3 crystallites which were grown on the monolayer. It is interesting to note that the peak assigned to the reduction of the amorphous tungsten species, for a loading near one monolayer, occurs on the γ-Al_2O_3 systems (23, 26, 39) at higher temperature than on the α-Al_2O_3 system described in this paper. This observation suggests that the use of an α-alumina support decreases the tungsten oxide–alumina interaction as compared to the γ-phase.

The second TPR patterns of the 6.7WA catalyst (Fig. 4), obtained after a first TPR followed by an oxidizing treatment in air at 400°C, are quite different from the first ones. They show four peaks at 380, 640, 732, and 855°C, similar to the TPR profiles of bulk WO_3. The consumption of hydrogen is $\Delta RN = 2.0$. The differences observed in the shape of the first and the second TPR profiles revealed that the oxidizing treatment of the reduced tungstate species led to the formation of either WO_3 crystallites or at least tungsten oxide species octahedrally coordinated. In the same way, Parera *et al.* (41) showed from a WO_3/ZrO_2 system that octahedrally coordinated tungstate species required lower temperature to be reduced than tetrahedral tungstate species. The peaks at $T < 750$°C were also ascribed to the reduction of bulk-like WO_3 species formed in $WO_{3-x,(0<x<1)}$ oxides or of octahedrally coordinated tungsten oxide species; the peak at 830°C was assigned to the reduction of the $WO_{3-x,(0<x<1)}$ suboxides in W, in accordance with the kinetics reduction process of bulk WO_3 (Fig. 5).

XANES Analysis

We obtained further information about the structure of the surface tungsten oxide species by the XANES technique. Figure 6 shows the tungsten L_I-edge of the reference compounds Na_2WO_4, WO_2, and WO_3. The most striking difference between the spectra of these tungsten oxide compounds lies in the pre-edge region. There is an intense and sharp feature in Na_2WO_4, where the WO_4 groups have a regular tetrahedral symmetry (42), and only a shoulder in WO_3, formed with distorted octahedral WO_6 groups. The pre-edge in the tungsten L_I-edge of Na_2WO_4 is due to 2*s*–5*d* transitions. Such a transition is possible because of the mixing of tungsten *d* orbitals with oxygen *p* orbitals (43) and corresponds therefore to a transition $2s \rightarrow 5d(W) + 2p(O)$. The transition is forbidden in the case of an octahedral symmetry with a center of inversion. In the case of a tetrahedral symmetry, as in Na_2WO_4, the transition is allowed by the absence of a center of inversion, and an intense pre-edge peak is observed (Fig. 6). Any distortion of the ideal octahedral symmetry, as in WO_3, which removes the center of inversion allows *s*–*d* transitions too. However the pre-edge feature is, in this case, broader and less intense than the pre-edge peak for tetrahedral symmetry (Fig. 6). Other differences can be seen at the near-edge part of the spectra. Both tetrahedral and octahedral tungsten species are characterized by a set of three small peaks, but the relative heights of these peaks are different. Thus, the pre-edge peak and the near-edge region can be used to distinguish between tetrahedral and octahedral surface tungsten oxide species.

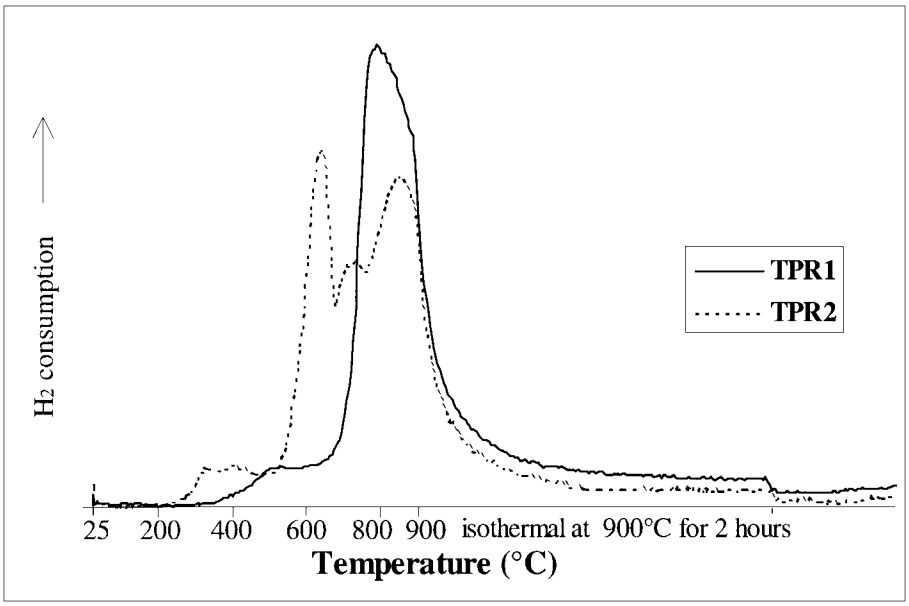

FIG. 4. TPR profiles of the 6.7WA catalyst.

Figure 7 shows the tungsten L_I-edge XANES of the 6.7WA catalyst calcined at 200°C, in a hydrogen-exposed sample at room temperature and in the same sample reduced *in situ* by hydrogen first at 450°C for 135 min then at 500°C for 90 min. Table 2 lists the energy shifts ΔE (eV) of the pre-edge peaks in the tungsten L_I-edges relative to the intense peak in the tungsten L_I-edge of Na_2WO_4 (12103.3 eV). The sharpness and the energy shift of the pre-edge peak of the tungsten L_I-edge of the 6.7WA sample at room temperature show a high degree of similarity to that of WO_3. By an *in situ* treatment in hydrogen at 450°C or 550°C, the energy position of the pre-edge feature is shifted towards lower energy and its intensity increases. At these temperatures, the near-edge region is characterized by one relatively broad peak and differs from those of the reference compounds WO_3 and Na_2WO_4. The observed changes in the tungsten L_I-edges of the 6.7WA catalyst with the *in situ* thermal treatment cannot be assigned to a reduction of the tungsten oxide species because a reduction of the hexavalent tungsten ions, in WO_3, to the

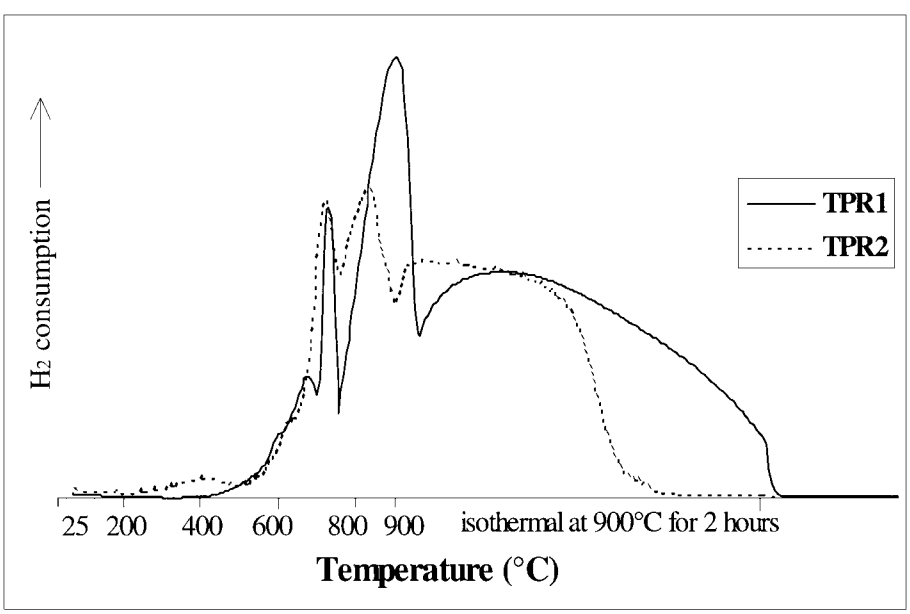

FIG. 5. TPR profiles of the bulk WO_3 catalyst.

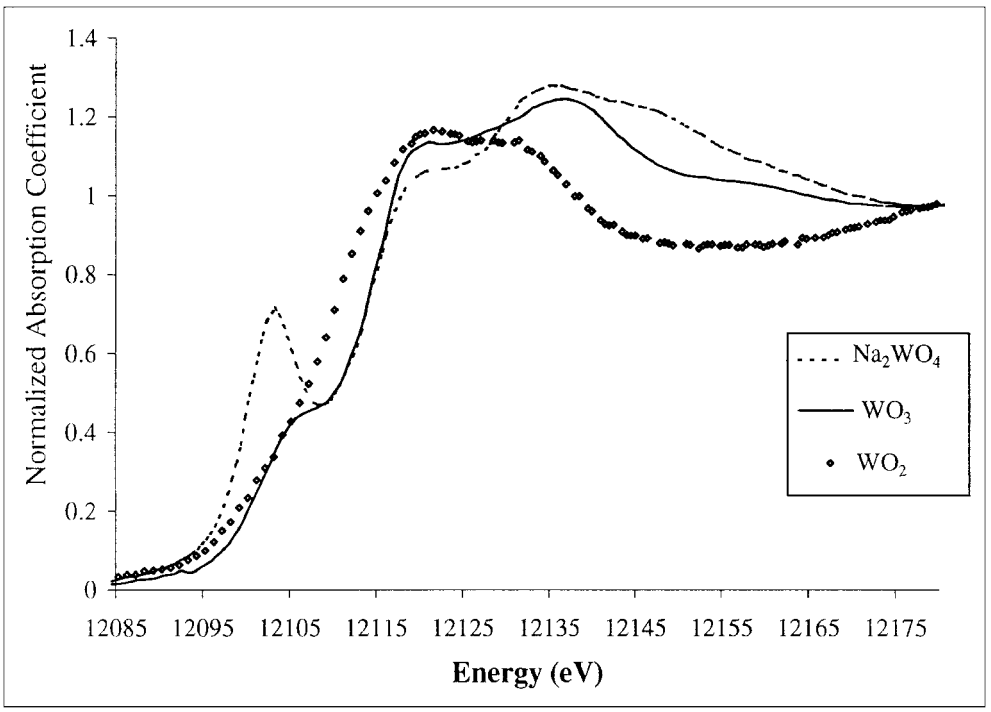

FIG. 6. Normalized tungsten L_I-edge XANES spectra for reference compounds Na_2WO_4, WO_3, and WO_2.

tetravalent tungsten ions, in the WO_2 oxide, leads to a removal of the pre-edge feature as shown in Fig. 6. The differences between the spectra for the room temperature exposed and heated 6.7WA sample are attributed to the removal of coordinated water molecules. Some works (24, 25, 44) have indeed shown that the addition of two water molecules to tetrahedral units would produce a pseudo-octahedral environment for the surface tungsten

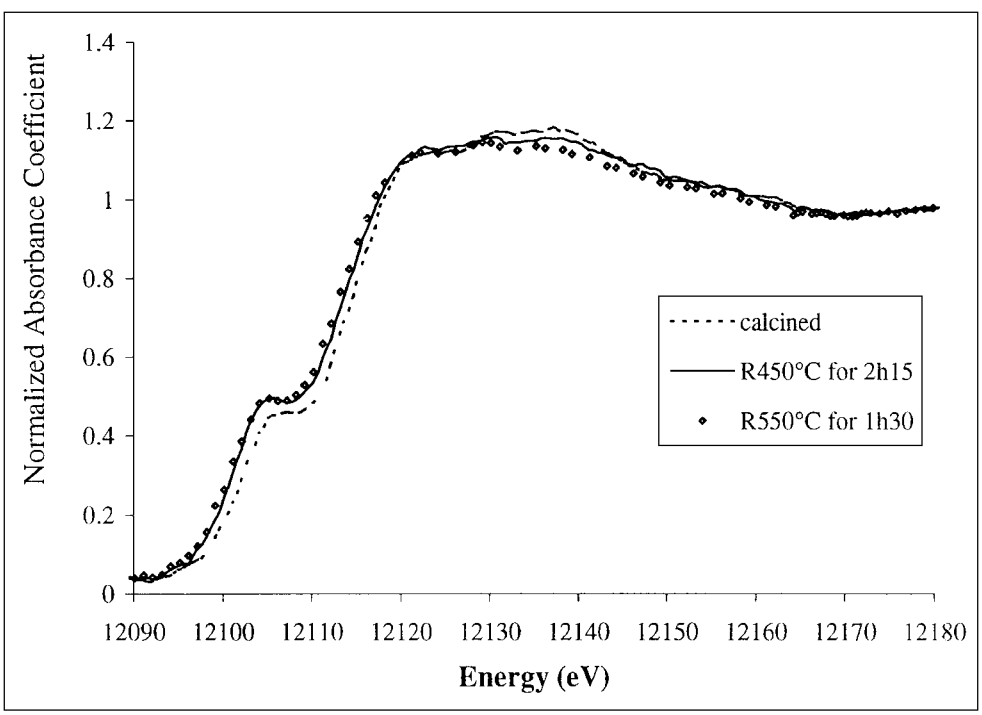

FIG. 7. Normalized tungsten L_I-edge XANES spectra for a 6.7WA sample calcined, then reduced in hydrogen at 450°C for 135 min then at 550°C for 1.5 h.

TABLE 2

Energy Shifts (ΔE) of the Pre-edge Peaks in the Tungsten L_I-Edges Relative to the Pre-edge Peak in the Tungsten L_I-Edge of Na_2WO_4

Sample	Treatment under H2 (temperature, °C)	ΔE (eV)
WO_3	RT	+2.3
6.7WA	RT	+2.3
6.7WA	450	+1.4
6.7WA	550	−1.4

oxide species, resulting in a pre-edge peak of reduced intensity. Using the XANES technique, Hilbrig *et al.* (44), who studied the structure of the surface tungsten species onto WO_x/TiO_2 systems for various tungsten oxide loadings, have obtained similar results to ours when the tungsten oxide coverage is about one monolayer. These authors proposed that the tungsten oxide species supported on TiO_2 consist of linked chains of WO_5 groups terminated by WO_4 species. According to the tungsten L_I-edges of the reference compounds and in agreement with the conclusions of Hilbrig *et al.* (44), we proposed that the surface tungsten oxide species on α-Al_2O_3, in the absence of coordinated water, is present as both WO_5 and WO_4 groups with a large majority of WO_5 groups because of the high coverage of tungsten oxide on our 6.7WA catalyst (about one monolayer). The 6.7WA sample exposed at room temperature has coordinated water molecules producing a pseudo-octahedral site symmetry, but the water molecules are removed by heating to 450°C. The XANES spectrum obtained after *in situ* thermal treatment by hydrogen does not reveal any reduction of the tungsten oxide species. This result confirms the low concentration of WO_3 crystallites at the surface up to the monolayer observed by the XPS measurements.

Catalytic Results

The conversion (α%) and the total selectivity in isomerized products (Siso%) obtained for the 4-methyl-1-pentene (4M1Pene) reactant on a 6.7WA sample are presented in Table 3 as a function of the time of exposure under hydrogen at 450°C. The sample was heated up from room temperature to the reaction temperature (350°C) in a helium stream. The helium stream is then replaced by a hydrogen stream and the first catalytic test is performed by introduction of the reactant by a pulse of 5 μl. The reaction temperature (350°C) is voluntarily selected for comparisons with other data from the laboratory (6, 8–10, 46, 47). Between two pulses of 4M1Pene, the surface is maintained at 450°C under the hydrogen stream. The distribution of the reaction products is summarized in Table 3. As observed, this catalyst shows very stable activity and selectivity under our conditions of treatment. The activity obtained during the first catalytic test reveals that no prereduction treatment of the catalyst is necessary to induce skeletal isomerization activity in contrast with what was observed on bulk tungsten oxides (8–10) or supported catalysts with a tungsten loading above one monolayer presenting large-sized WO_3 crystallites at the surface (9, 18, 22). The global selectivity in isomerized products is about 97% and the main product formed is the 3MP (∼61%). Lower amounts of 23DMB and *n*H are produced, about 16 and 19%, respectively. This distribution of isomerized products (Table 3) leads to a 3MP/*n*H ratio close to 3.4, which is representative of an acidic behaviour. Traces of 22DMB are formed, but no cyclic products are detected. This excludes the contribution of a cyclic mechanism to isomerization, which occurs on classical Pt/Al_2O_3 catalysts (45). Among the cracked products, C3 is mainly formed and C1 and C2 are negligible. This cracking distribution seems to confirm that the 6.7WA catalyst exhibits acidic catalytic properties only.

The conversion α% and the reaction product distribution obtained for the 1-hexene (1Hene), cyclohexene (CHene), and methylcyclopentene-1 (MCPene) reactants on the 6.7WA samples at 350°C under a hydrogen stream are reported, respectively, in Tables 4, 5, and 6. Between two pulses of reactant, the samples are maintained at 350°C under the hydrogen stream. It is important to note, as mentioned previously in the experimental part, that the reaction products are hydrogenated before analysis.

The distribution of the C6 isomers for the 1Hene reactant (Table 4) shows a high selectivity in monobranched molecules (2MP and 3MP) since they represent approximately 82% of the isomers. Among the cracked products, C3 is mainly formed. As for the 4M1Pene reaction, no cyclic products are formed. The CHene reactant is mainly transformed in MCP (Table 5) and almost no cracking of the ring is observed. MCP undergoes mainly ring enlargement

TABLE 3

Activity and Selectivity of 4M1Pene Reaction on a 15-mg 6.7WA Sample at 350°C as a Function of Time of Exposure at 450°C under Hydrogen

Time (h)	0.1	1	2	3	5	15
α(%)	52.4	56.8	58.4	58.6	57.8	58
Siso(%)	98.8	96.4	96.8	95.9	97.0	97.6
C1	—	0.3	—	0.1	0.1	0.1
C2	—	—	—	—	0.2	0.1
C3	0.7	1.5	1.4	1.5	1.3	1.2
*i*C4 + *n*C4	0.3	1.0	1.0	1.2	0.8	0.5
*i*C5 + *n*C5	0.2	0.8	0.8	1.0	0.6	0.5
22DMB	0.7	0.6	0.6	0.7	0.6	0.6
23DMB	12.9	16.4	15.9	16.2	15.8	15.6
3MP	71.4	62.8	60.9	59.5	61.5	63.1
*n*H	13.8	16.6	19.4	19.8	19.1	18.3
3MP/*n*H	5.2	3.8	3.1	3.0	3.2	3.5

TABLE 4

Activity and Selectivity of nHene Reaction on a 15-mg 6.7WA Sample at 350°C

Test	1	2	3
α(%)	70.4	70.2	69.5
Siso(%)	94.7	94.8	95
C1	0.5	0.4	0.5
C2	0.4	0.4	0.4
C3	2.3	2.1	1.9
iC4 + nC4	1.3	1.4	1.3
iC5 + nC5	0.8	0.9	0.9
22DMB	0.6	0.6	0.6
23DMB	12.2	12.2	12.1
2MP	43.1	43.1	43.1
3MP	38.8	38.9	39
2MP/3MP	1.1	1.1	1.1

giving CH (Table 6). We can observe a decrease in the ring enlargement of MCP in favour of extensive cracking in methane for the successive catalytic tests while the total conversion remains constant. We attribute this distribution modification to the formation of carbonaceous residues, as it is well known that MCP is a poison for acidic sites (45).

We note the surprising and interesting stability of this catalyst under the hydrogen stream as compared to the bulk tungsten oxides WO_3 and WO_2 (8–10), which exhibit an evolution from an acidic to a metallic catalytic behaviour as a function of time of exposure under a hydrogen stream. This was correlated to the progressive reduction of the surface oxide species from WO_3 to metal W. The remarkably stable catalytic behaviour of the 6.7WA sample suggests that no modification of the nature of the active phase occurs during its exposure under the hydrogen stream at 450°C. As a consequence, these results are in agreement with those of the characterization data described above, and we attributed the catalytic activity and remarkable selectivity in skeletal isomerization of 4M1Pene and 1Hene, in MCP from CHene and in ring enlargement of MCP, to the presence of the amorphous tetra- or penta-coordinated tungsten oxide species. The product distributions indicate that the reaction proceeds through a monofunctional acidic mechanism. Carbenium ions are involved as reaction intermediates leading to surface alkoxy species, as earlier proposed on bulk tungsten carbide surfaces modified by chemisorbed oxygen (6, 7). The carbenium ions can be formed either by protonation of the reactant by Brønsted acidic sites as OH groups or by hydride abstraction by Lewis acidic sites as W^{6+} ions. It is important to note that this 6.7WA catalyst is totally inactive for alkane reactants whatever the time of exposure of the sample under a hydrogen stream at 450°C. This inactivity of the surface for alkane isomerization reveals an absence of metallic dehydrogenation sites. This absence of dehydrogenation sites despite the formation of W^0 species resulting from the reduction of the few WO_3 crystallites present up to the monolayer, as observed by XPS after a thermal treatment under hydrogen at 450°C, is attributed to a rapid poisoning of these tungsten metal species by the reactant stream. This suggestion is supported by previous work realized in the laboratory (46, 47) which has shown that clean tungsten metal surfaces are rapidly poisoned by hydrocarbons.

TABLE 5

Activity and Selectivity of CHene Reaction on a 15-mg 6.7WA Sample at 350°C

Test	1	2	3
α(%)	79.6	78.8	79.6
C1 + C2 + C3	0.3	0.2	0.4
C4	0.4	0.4	0.4
C5	0.3	0.2	0.2
CP	0.1	0.1	0.1
MCP	98.8	99	98.8

TABLE 6

Activity and Selectivity of MCPene Reaction on a 15-mg 6.7WA Sample at 350°C

Test	1	2	3
α(%)	8.5	8.0	8.5
C1	4.5	17.4	26.6
C2	0.8	0.7	2.0
C3	1.7	1.1	1.2
iC4 + nC4	4.9	2.4	2.0
iC5 + nC5	3.3	1.1	1.0
CP	0.5	0.7	0.5
2MP + 3MP	1.2	0.4	0.5
CH	82.7	76.2	66.2

A catalytic test using 4M1Pene under a helium stream, instead of a hydrogen stream, has been performed on a fresh calcined 6.7WA sample. This test reveals that the initial surface is active ($\alpha\% = 32\%$) and very selective in skeletal isomerization (Siso% = 91%) of 4M1Pene. The selectivity in 3MP is more important (~76.6%) when the catalytic test is performed under helium than under a hydrogen stream (Table 3) while 23DMB and nH are produced in lower amounts, 6.4 and 6.1%, respectively. These changes in the isomerized product distribution with the nature of the gas stream (H_2 or He) is attributed to a modification of the nature or the strength of the acidic sites. Soled *et al.* (27) have reported already that surface WO_3 groups coordinate with either one or two alumina surface OH groups forming either a Lewis or a Brønsted site. These Lewis or Brønsted sites could assume, respectively, the configurations represented in Schemes 1a and 1b. It was suggested that an increase of the WO_3 loading and/or the calcination temperature favours the configuration 1b over 1a. The low

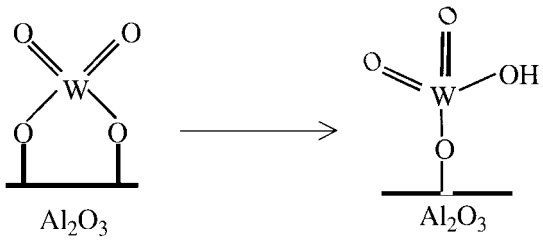

SCHEME 1

calcination temperature (200°C) used in the case of the 6.7WA preparation leads us to postulate that mainly Lewis acidic sites are formed compared to Brønsted acidic sites. The acidic character of the fresh calcined surface is thus mainly attributed to the presence of the hexavalent tungsten ions, in the WO_5 and WO_4 groups which composed the surface, as Lewis acidic sites. Ponec *et al.* (21), who studied by IR spectroscopy the surface properties of supported tungsten oxide catalysts and the interaction of these catalysts with *n*-butenes, proposed that the presence on the surface of both Brønsted and Lewis acidic sites is necessary to develop a selective catalyst for the isomerization of *n*-butene to isobutene. In agreement with these authors, we suggest that the Lewis acidic W^{6+} sites are responsible for the adsorption of the reactant on the surface while the Brønsted sites account for the skeletal isomerization itself. To explain the increase in the total activity and the few modifications in the distribution of isomer products when helium is replaced by hydrogen, we suggest that a transformation of some Lewis W^{6+} sites, present in the terminal WO_4 groups, into Brønsted acidic sites by interaction with hydrogen atoms occurs under hydrogen.

It is worthwhile to mention that the 6.7WA catalyst is more easily poisoned by hydrocarbons (4M1Pene, 1Hene, Chene) at low temperature (200°C) compared to 350°C (Table 7). However, a simple heating of the catalyst under hydrogen at 350°C is enough to recover both the initial activity and the initial selectivity. The poisoning observed at low temperature is attributed to the formation of carbonaceous species which can be reversibly hydrogenated at higher temperature (350°C).

TABLE 7

Activity and Selectivity of 4M1Pene Reaction on a 15-mg 6.7WA Sample at 200°C as a Function of Time of Exposure at 200°C under Hydrogen

Time (min)	0	30	60	90	120
α(%)	31.1	31.0	25.4	22.8	21.3
Siso(%)	95	95.2	97.3	97.5	97.8
C1 + C2 + C3	0.9	0.8	0.6	0.8	0.5
*i*C4 + *n*C4	1.7	1.6	0.8	0.8	0.6
*i*C5 + *n*C5	2.3	2.4	1.3	0.9	1.1
22DMB	0.1	0.2	0	0	0
23DMB	4.4	4.6	3.7	3.2	3.5
3MP	87.9	88.0	91.5	91.9	92.2
*n*H	2.6	2.4	2.1	2.4	2.1
3MP/*n*H	33.8	36.7	43.6	38.3	43.9

CONCLUSION

Porous monoliths of α-alumina, prepared by a novel method, have been used as supports for a catalyst containing tungsten oxide, with a coverage approaching a monolayer. This catalyst exhibits high and very stable activity and isomer selectivity under the hydrogen stream at 350°C or higher temperature. No prereduction of the surface is necessary to induce skeletal isomerization; this WO_3/α-Al_2O_3 system is indeed active under a helium stream. Whatever the nature of the gas stream, the isomerization always proceeds through an acidic mechanism involving carbenium ion rearrangements.

The characterization of the sample indicates that the surface is mainly formed by amorphous tungsten oxide species, composed of WO_5 and tetrahedral WO_4 groups, which strongly interact with the alumina support and are irreducible under our catalytic conditions (temperature, pressure, and time under hydrogen). Some WO_3 crystallites, which are reduced via the same mechanism and conditions as bulk WO_3, have been detected on top of amorphous alumina-supported tungsten oxide species.

As underlined by one referee, it is well known that supported oxide catalysts can undergo structural changes during a start-up regime of a catalytic reaction. We should emphasize (thanks to the reviewer) that all the characterizations reported are for the catalyst prior to the catalytic reaction and that our correlations between catalytic and structural characteristics hold perhaps only for a "precursor" state.

However, we can note that no induction period under continuous flow conditions is required to obtain skeletal isomerization. So the remarkable isomerization activity and stability of this catalyst has been attributed to the amorphous species. The WO_3 crystallites have no activity in the hexene isomerization because of their rapid poisoning by the reactant stream. Such a catalyst is less resistant to poisoning by carbonaceous residues at low temperature (200°C), but is fully rejuvenated by simple exposure to hydrogen at 350°C.

ACKNOWLEDGMENTS

The authors thank Dr. D. Bazin and Dr. R. Revel (LURE, Orsay) for assistance with XANES experiments.

REFERENCES

1. Ribeiro, F., Dalla Betta, R., Boudart, M., Baumgartner, J., and Iglesia, E., *J. Catal.* **130**, 86 (1991).

2. Ribeiro, F., Boudart, M., Dalla Betta, R., and Iglesia, E., *J. Catal.* **130**, 498 (1991).
3. Iglesia, E., Baumgartner, J., Ribeiro, F., and Boudart, M., *J. Catal.* **131**, 523 (1991).
4. Frennet, A., Leclercq, G., Leclercq, L., and Maire, G., *et al.*, *in* "Proceedings, 10th International Congress on Catalysis, Budapest, 1992" (L. Guczi, F. Solymosi, and P. Tetenyi, Eds.), Akadémìai Kiado, Budapest, 1993.
5. Keller, V., Wehrer, P., Garin, F., Ducros, R., and Maire, G., *J. Catal.* **153**, 9 (1995).
6. Keller, V., Wehrer, P., Garin, F., Ducros, R., and Maire, G., *J. Catal.* **166**, 125 (1997).
7. Garin, F., Keller, V., Ducros, R., Muller, A., and Maire, G., *J. Catal.* **166**, 136 (1997).
8. Katrib, A., Logie, V., Peter, M., Wehrer, P., Hilaire, L., and Maire, G., *J. Chim. Phys.* **94**, 1923 (1997).
9. Logie, V., Ph.D. Thesis, ULP Strasbourg, France, 1998.
10. Bigey, C., Logie, V., Bensaddik, A., Schmitt, J. L., and Maire, G., *in* "Journal de Physique IV" (A. Cornet and N. Broll, Eds.), Proceedings, *Rayons X et Matière*, Vol. 8, p. 553, 1998.
11. Salvati, L., Makovsky, L., Stencel, J., Brown, F., and Hercules, D., *J. Phys. Chem.* **85**, 3700 (1981).
12. Tittarelli, P., Iannibello, A., and Villa, P., *J. Solid State Chem.* **37**, 95 (1981).
13. Grünert, W., Shpiro, E., Feldhaus, R., Anders, K., Antoshin, G., and Minachev, K., *J. Catal.* **107**, 522 (1987).
14. Wachs, I., Chersich, C., and Hardenberg, J., *Appl. Catal.* **13**, 335 (1985).
15. Biloen, P., and Pott, G., *J. Catal.* **30**, 169 (1973).
16. Thomas, R., Kerkhof, G., and Moulijn, J., *J. Catal.* **61**, 559 (1980).
17. Gielgens, L., Van Kampen, M., Broek, M., van Hardeveld, R., and Ponec, V., *J. Catal.* **154**, 201 (1995).
18. Baker, B., and Clark, N., *in* "Catalysis and Automotive Pollution Control" (A. Crucq and A. Frennet, Eds.), Studies in Surface Science and Catalysis, Vol. 30, p. 483. Elsevier, Amsterdam, 1987.
19. Chapell, P., Kibel, M., and Baker, B., *J. Catal.* **110**, 139 (1988).
20. Baker, B., and Jasieniak, J., *in* "Surface Science: Principles and Applications" (R. Howe, R. Lamb, and K. Wandelt, Eds.), Springer Proceedings in Physics, Vol. 73, p. 279. Springer-Verlag, Berlin/Heidelberg, 1993.
21. Meijers, S., Gielgens, L., and Ponec, V., *J. Catal.* **156**, 147 (1995).
22. Chan, S., Wachs, I., Murrell, L., and Dispenziere, N., *J. Catal.* **92**, 1 (1985).
23. Thomas, R., Van Oers, E., De Beer, V., Medema, J., and Moulijn, J., *J. Catal.* **76**, 241 (1982).
24. Chan, S., Wachs, I., Murrell, L., Wang, L., and Hall, W., *J. Phys. Chem.* **88**, 5831 (1984).
25. Horsley, J., Wachs, I., Brown, J., Via, G., and Hardcastle, F., *J. Phys. Chem.* **91**, 4014 (1987).
26. Vermaire, D., and Van Berge, P., *J. Catal.* **116**, 309 (1989).
27. Soled, S., Mc Vicker, G., Murrell, L., Sherman, L., Dispenziere, N., Hsu, S., and Waldman, D., *J. Catal.* **111**, 286 (1988).
28. Vignes, J. L., Mazerolles, L., and Michel, D., *in* "Key Engineering Materials," Vols. 132–136, p. 432. Trans. Tech. Publications, Switzerland, 1997.
29. Romeo, M., Bak, K., El Fallah, J., Hilaire, L., and Maire, G., *J. Elec. Spec.* **76**, 195 (1995).
30. Monti, D., and Baiker, A., *J. Catal.* **83**, 323 (1983).
31. Malet, P., and Caballero, A., *J. Chem. Soc. Faraday Trans. I* **84**, 2369 (1988).
32. Michalowicz, A., *in* "Logiciel pour la chimie," p. 116. Société Française de Chimie, Paris, 1991. ["EXAFS pour MAC"]
33. Katrib, A., Hemming, F., Wehrer, P., Hilaire, L., and Maire, G., *Topics Catal.* **1**, 75 (1994).
34. Kadkhodayan, A., and Brenner, A., *J. Catal.* **117**, 311 (1989).
35. Thomas, R., and Mouljin, J., *J. Mol. Catal.* **15**, 157 (1982).
36. Schubert, W., *Int. J. Refract. Hards Metals* **9**(4), 178 (1990).
37. Lavrenko, V., Zenkov, V., Tikush, V., and Uvarova, I., *Russ. J. Phys. Chem.* **50**, 706 (1976).
38. Ogata, E., Kamiya, Y., and Ohto, N., *J. Catal.* **29**, 296 (1973).
39. De Angelis, B., and Schiavello, M., *J. Solid State Chem.* **21**, 67 (1997).
40. Kadkhodayan, A., and Brenner, A., *J. Catal.* **117**, 311 (1989).
41. Yori, J., Vera, C., and Parera, J., *Applied Catal.* **163**, 165 (1997).
42. Okada, K., Morikawa, H., Marumo, F., and Iwai, S., *Acta Crystallogr.* **B30**, 1872 (1974).
43. Kutzler, F., Natoli, C., Misemer, D., Doniach, S., and Hodgson, K., *J. Chem. Phys.* **73**, 3274 (1980).
44. Hilbrig, F., Göbel, H., Knözinger, H., Schmelz, H., and Lengeler, B., *J. Phys. Chem.* **95**, 6973 (1991).
45. Gault, F., *Adv. Catal.* **30**, 1 (1981).
46. Wanner, S., Hemming, F., Wehrer, P., Hindermann, J. P., and Maire, G., *Bull. Soc. Chim. Belg.* **105**, 121 (1996).
47. Hemming, F., Wehrer, P., Katrib, A., and Maire, G., *J. Mol. Catal. A Chem* **124**, 39 (1997).